Abrogation of MAPK and Akt Signaling by AEE788 Synergistically Potentiates Histone Deacetylase Inhibitor-Induced Apoptosis through Reactive Oxygen Species Generation

Chunrong Yu,[1] Bret B. Friday,[1] Jin-Ping Lai,[3] Andrea McCollum,[2] Peter Atadja,[4] Lewis R. Roberts,[3] and Alex A. Adjei[5]

Abstract

Purpose: To evaluate the effects of combining the multiple receptor tyrosine kinase inhibitor AEE788 and histone deacetylase (HDAC) inhibitors on cytotoxicity in a broad spectrum of cancer cell lines, including cisplatin-resistant ovarian adenocarcinoma cells.

Experimental Design: Multiple cancer cell lines were treated *in vitro* using AEE788 and HDAC inhibitors (LBH589, LAQ824, and trichostatin A), either alone or in combination. Effects on cytotoxicity were determined by growth and morphologic assays. Effects of the combination on cell signaling pathways were determined by Western blotting, and the results were confirmed using pathway-specific inhibitors and transfection of constitutively active proteins.

Results: Cell treatment with AEE788 and HDAC inhibitors (LBH589, LAQ824, and trichostatin A) in combination resulted in synergistic induction of apoptosis in non–small cell lung cancer (MV522, A549), ovarian cancer (SKOV-3), and leukemia (K562, Jurkat, and ML-1) cells and in OV202hp cisplatin-resistant human ovarian cancer cells. AEE788 alone or in combination with LBH589 inactivated mitogen-activated protein kinase (MAPK) and Akt cascades. Inhibition of either MAPK and/or Akt enhanced LBH589-induced apoptosis. In contrast, constitutively active MAPK or Akt attenuated LBH589 or LBH589 + AEE788–induced apoptosis. Increased apoptosis was correlated with enhanced reactive oxygen species (ROS) generation. The free radical scavenger *N*-acetyl-L-cysteine not only substantially suppressed the ROS accumulation but also blocked the induction of apoptosis mediated by cotreatment with AEE788 and LBH589.

Conclusion: Collectively, these results show that MAPK and Akt inactivation along with ROS generation contribute to the synergistic cytotoxicity of the combination of AEE788 and HDAC inhibitors in a variety of human cancer cell types. This combination regimen warrants further preclinical and possible clinical study for a broad spectrum of cancers.

AEE788 is a 7*H*-pyrrolopyrimidine that inhibits the tyrosine kinase activity of the vascular endothelial growth factor receptor (VEGFR), epidermal growth factor receptor (EGFR), HER-2/*neu* (ErbB2), and other kinases including c-src, c-abl, c-fms, and flt-1 (1). An oral formulation of AEE788 is currently in phase I clinical development. In preclinical studies, AEE788 showed high target specificity and showed antiproliferative effects in tumor cell lines and in animal models of cancer. AEE788 has been shown to concomitantly inhibit EGFR and VEGFR2 *in vitro* and *in vivo* and consequently abrogates multiple survival signaling pathways, including mitogen-activated protein kinase (MAPK) and Akt, in a dose-dependent fashion (2–4). The MAPK family mainly consists of the extracellular signal-regulated kinase 1/2 (Erk1/2), c-Jun NH_2-terminal kinase, and p38 MAPK kinase members (5, 6). Whereas c-Jun NH_2-terminal kinase and p38 MAPK activities are involved in proapoptotic events (7), activation of the Erk1/2 pathway occurs via activation of Ras at the plasma membrane, which is classically followed by sequential activation of the Raf family of kinases, followed by MAP/Erk kinase 1/2 (MEK1/2) and then Erk1/2. Activated Erk1/2 then phosphorylates various downstream substrates involved in a multitude of cellular responses, such as cell proliferation, cell differentiation, and cell survival (8, 9). The relevance of the Erk1/2 cascade in human malignancies is shown by the frequency of activating mutations among its constituents. Ras mutations are found in ~30% of known human tumors, and BRAF mutations are common in melanomas and thyroid malignancies (10–12). Similarly, the components of the phosphatidylinositol 3-kinase (PI3K)/Akt signaling pathway are frequently altered in cancer and have been shown to induce malignant transformation and chemoresistance (13).

Histone deacetylases (HDAC) and histone acetyltransferases regulate gene expression by removal or addition, respectively,

Authors' Affiliations: Departments of [1]Oncology and [2]Molecular Pharmacology and [3]Division of Gastroenterology and Hepatology, Mayo Clinic, Rochester, Minnesota; [4]Novartis Institutes for Biomedical Research, Boston, Massachusetts; and [5]Department of Medicine, Roswell Park Cancer Institute, Buffalo, New York

Received 7/18/06; revised 9/20/06; accepted 10/31/06.

The costs of publication of this article were defrayed in part by the payment of page charges. This article must therefore be hereby marked *advertisement* in accordance with 18 U.S.C. Section 1734 solely to indicate this fact.

Requests for reprints: Alex A. Adjei, Department of Medicine, Roswell Park Cancer Institute, Elm and Carlton Streets, Buffalo, NY 14263. Phone: 716-845-4101; Fax: 716-845-3423; E-mail: alex.adjei@roswellpark.org.

doi:10.1158/1078-0432.CCR-06-1751

of acetyl groups to ε-amino groups in lysine residues of core nucleosomal histones (14). HDAC inhibitors constitute a diverse group of compounds that promote histone acetylation; chromatin uncoiling; deacetylation of transcription factors, such as p53, GATA-1, TFIIE, and TFIIF; and transcription of a variety of genes, such as the cell cycle regulators *p21* and *p27*, which are involved in multiple cellular processes, including differentiation (15). This class of drugs induces apoptosis through a process regulated by induction of the cyclin-dependent kinase inhibitor $p21^{CIP1}$ (16) or generation of reactive oxygen species (ROS) and cleavage of Bid (17).

ROS are constantly generated and eliminated in biological systems (18, 19). Dysregulation of electron transport through the mitochondrial respiratory chain or impairment in the function of antioxidant enzymes results in the accumulation of ROS. Under various pathologic conditions such as ischemia, excessive amounts of accumulated ROS induce apoptosis or necrosis by activating the MAPK and caspase cascades and/or by disrupting mitochondrial membrane potential (20). This contribution of ROS to apoptosis and necrosis is highly cell type specific and also depends on the amount of endogenously or exogenously generated ROS present. Alternatively, ROS may act directly on the mitochondria to induce the mitochondrial membrane permeability transition, which results in the release of apoptogenic factors such as cytochrome *c*, apoptosis-inducing factor, and/or Smac/DIABLO (21–27). Other reported actions of ROS include up-regulation of death receptors such as tumor necrosis factor–related apoptosis-inducing ligand, Fas ligand, and Fas (28–30); interruption of heat shock protein 90 function (31); and expression of caspase-8 and/or regulation of Bcl-2 family members (32).

LBH589 is a pan-HDAC inhibitor at nanomolar concentrations (IC_{50}: HDAC1 at 6 nmol/L, HDAC3 at 1 nmol/L, HDAC4 at 9 nmol/L, HDAC5 at 3 nmol/L, and HDAC6 at 6 nmol/L). It is a cinnamic hydroxamic acid lactate salt that increases histone H3 and H4 acetylation levels, the hallmark of target modulation, in treated tumor cells both *in vitro* and *in vivo* (33). Safety and tolerability have been shown in a preliminary report of an ongoing phase I study in patients with solid tumors or lymphoma. Common toxicities include nausea, diarrhea, fatigue, anorexia, dysgeusia, and thrombocytopenia (34).

Previous studies have shown that interruption of signaling pathways, including the MAPK and PI3K/Akt cascades, the Bcr/Abl pathway, or proteasome activity, can lower the threshold for HDAC inhibitor–induced cancer cell lethality (35–41). Because AEE788 has been shown to inhibit EGFR, VEGFR2, MAPK, and Akt activity, we hypothesized that combining AEE788 with HDAC inhibitors would lead to synergistic cytotoxicity in cancer cells. This study investigated the cytotoxic attributes of the combination of AEE788 with HDAC inhibitors in human cancer cells and the underlying molecular basis of the observed results. Our study shows that AEE788 synergistically potentiates HDAC inhibitor–induced apoptosis in a broad spectrum of solid tumor and leukemia cell lines as well as cisplatin-resistant human ovarian cancer cells. Moreover, we have shown that inactivation of the MAPK and Akt pathways as well as generation of ROS play a crucial role in the synergistic cytotoxicity arising from the combination of AEE and HDAC inhibitors in tumor cells.

Materials and Methods

Cells. A549, SKOV-3, MIA, ML-1, and Jurkat cell lines were purchased from the American Type Culture Collection (Manassas, VA). K562 cells was purchased from DSMZ-Deutsche Sammlung von Mikroorganismen und Zellkulturen GmbH (Braunschweig, Germany). MV522 cells were obtained from Dr. Julian Molina (Mayo Clinic, Rochester, MN). and have been previously described (42). OV202hp cells, patient derived ovarian cancer cells, have been previously described (43). All cells were grown following instructions provided by suppliers.

Cell culture. Subconfluent, logarithmically growing cells were placed in sterile plastic T-flasks, allowed to adhere, supplemented with the designated drugs, and incubated in a humidified incubator with 5% CO_2 at 37°C for various time intervals as indicated.

Materials. AEE788, LBH589, and LAQ824 were kindly provided by Dr. Peter Atadja (Novartis Pharmaceuticals, Basel, Switzerland). Agents were purchased from the following suppliers: U0126 from BioMol Research Laboratories (Plymouth, MA) and trichostatin A from Sigma Chemical Co. (St. Louis, MO).

Assessment of apoptosis. After drug exposure, apoptotic cells were detected by 4′,6-diamidino-2-phenylindole dihydrochloride staining, which allowed identification of apoptotic nuclear changes as described previously (38). Briefly, cells were washed with PBS and fixed with 1% glutaraldehyde at room temperature for 30 min. After washing with PBS, cells were resuspended in 20 μL of PBS and mixed with 5 μL of 10 μg/mL 4′,6-diamidino-2-phenylindole dihydrochloride. Cell suspensions were mounted on slides and subjected to fluorescence microscopic examination. To confirm the morphologic results, Wright-Giemsa stains were done. In brief, after drug treatment, cells were transferred to slides by cytocentrifugation, fixed, stained, and evaluated under light microscopy for apoptotic cells. Apoptotic cells were identified by classic morphologic features (i.e., nuclear condensation, cell shrinkage, and formation of apoptotic bodies). Five or more randomly selected fields, encompassing a total of ≥500 cells per slide, were quantified for the percentage of apoptotic cells. To further confirm the results of morphologic analysis, Annexin/propidium iodide (BD PharMingen, San Diego, CA) analysis was carried out as per manufacturer's instruction.

Immunoblot analysis. Cell lysates were prepared and subjected to immunoblot analysis using 30 μg of cellular protein using standard techniques, following drug treatment. The sources of primary antibodies were as follows: caspase-9 (rabbit polyclonal), cleaved caspase-3 (rabbit polyclonal), Bid (rabbit polyclonal), poly(ADP-ribose) polymerase (PARP; mouse monoclonal), phosphorylated Erk1/2 (Thr^{202}/Tyr^{204}; rabbit polyclonal), phosphorylated p38 (Thr^{180}/Tyr^{182}; rabbit polyclonal), phosphorylated c-Jun NH_2-terminal kinase (mouse monoclonal), phosphorylated Akt (rabbit polyclonal), phosphorylated glycogen synthase kinase-3β (rabbit polyclonal), phosphorylated p70S60K (rabbit polyclonal), Akt (rabbit polyclonal), Erk1/2 (rabbit polyclonal) from Cell Signaling Technology (Beverly, MA); caspase-8 (mouse monoclonal) from AXXORA, LLC (San Diego, CA); cytochrome *c* (mouse monoclonal) from Santa Cruz Biotechnology (Santa Cruz, CA). To ensure equivalent loading and transfer, blots were stripped and reprobed with anti-actin antiserum. Western blots are representative of three independent experiments.

Assessment of cytochrome* c *release from mitochondria. Following drug treatment, the release of cytochrome *c* from mitochondria was analyzed by a selective digitonin permeabilization method. For these assays, 4×10^6 cells per condition were resuspended in 50 μL of permeabilization buffer [containing 75 mmol/L NaCl, 8 mmol/L Na_2PO_4, 1 mmol/L NaH_2PO_4 (pH 7.4), 250 mmol/L sucrose (added fresh before use), 1 mmol/L EDTA, 700 μg/mL digitonin; final concentration of digitonin 35 μg per 4×10^6 cells]. After incubation at room temperature for 1 min, cells were pelleted by centrifugation for 3 min at 13,000 × *g*, and the supernatants containing cytochrome *c* protein were obtained.

Measurement of ROS. ROS was detected by 5-(and-6)-chloromethyl-2′,7′-dichlorodihydrofluorescein diacetate (Molecular Probes, Eugene, OR) following the supplier's instructions. After this agent diffuses into cells and is sequestered intracellularly by de-esterification, subsequent reaction with peroxides generates fluorescent 5-chloromethyl-2′,7′-dichlorofluorescein. Briefly, following treatment, cells were collected by centrifugation, resuspended in PBS containing 10 μmol/L 5-(and-6)-chloromethyl-2′,7′-dichlorodihydrofluorescein diacetate, incubated for 1 h at 37°C, washed with PBS to remove unreacted dye, re-incubated in medium at 37°C for 10 min, read on the FL-1 channel of a Becton Dickinson FACSCalibur, and analyzed using CellQuest Software. The percentage of cells displaying increased dye uptake was used to reflect an increase in ROS levels.

Analysis of combined drug effects. The effect of combining AEE778 and LBH589 was analyzed using the median effect method of (44) using Calcusyn software (Biosoft, Oxford, United Kingdom) as reported previously (45).

Transient transfection. Constitutively active MEK1 (S218D/S222D) and myr-Akt1-myc (constitutively activated Akt1-myc) in pUSEamp (Upstate, Lake Placid, NY) were subcloned in-frame into the pEGFP

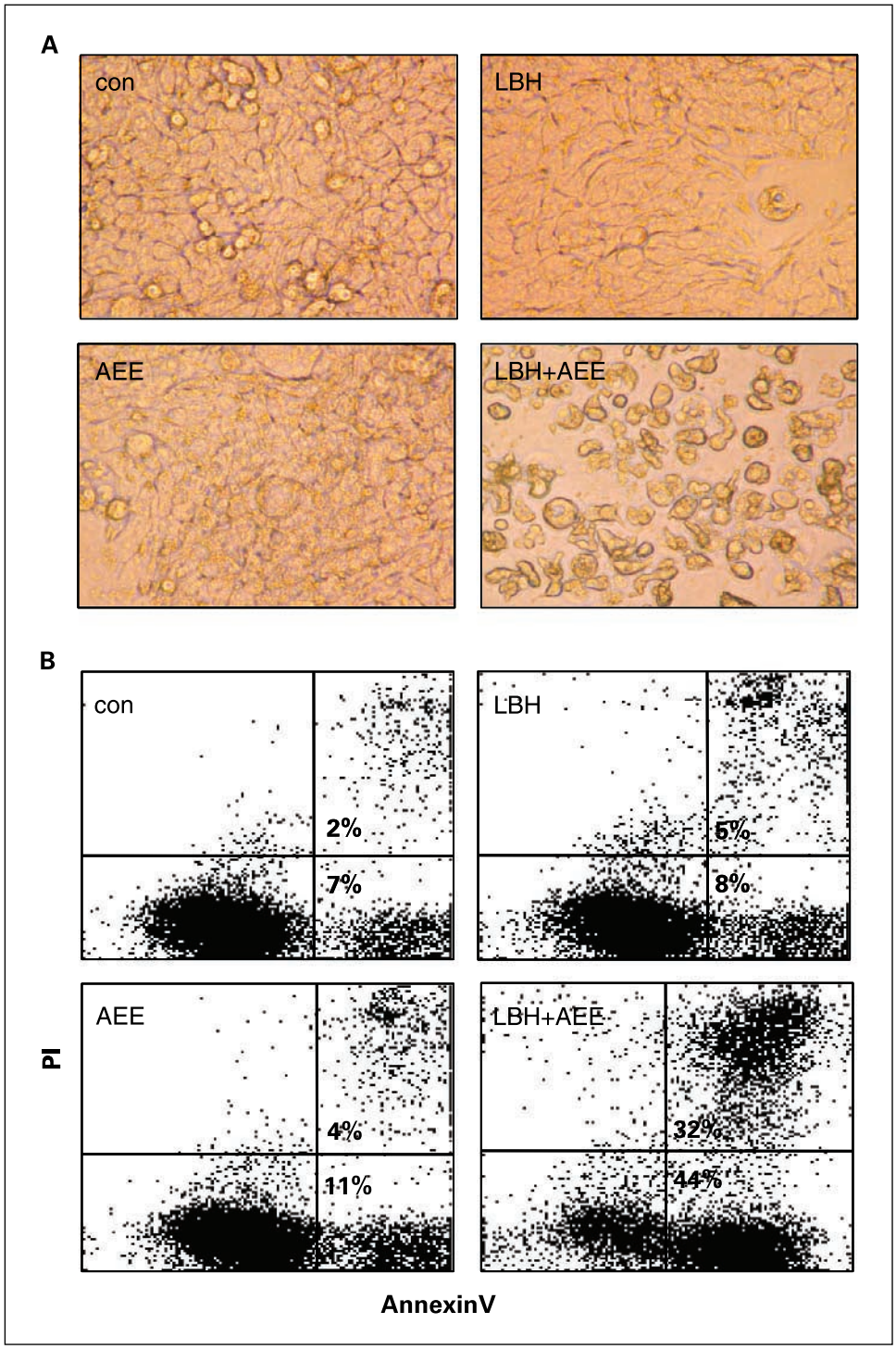

Fig. 1. Induction of enhanced cell death in MV522 and K562 cells after cotreatment of AEE788 and LBH589. *A,* MV522 cells were treated with 25 nmol/L LBH589 (*LBH*) and/or 1.0 μmol/L AEE788 (*AEE*) for 72 h. Morphology was determined using phase-contrast microscopy. *B,* after K562 cells were treated with 25 nmol/L LBH589 and/or 2.5 μmol/L AEE788 for 24 h, the extent of apoptosis was determined by flow cytometric analysis of Annexin V/propidium iodide staining. Cells in the lower right quadrant (Annexin V positive) represent early apoptotic cells; cells in the upper right quadrant (Annexin V/propidium iodide positive) represent later apoptotic cells. Con, control.

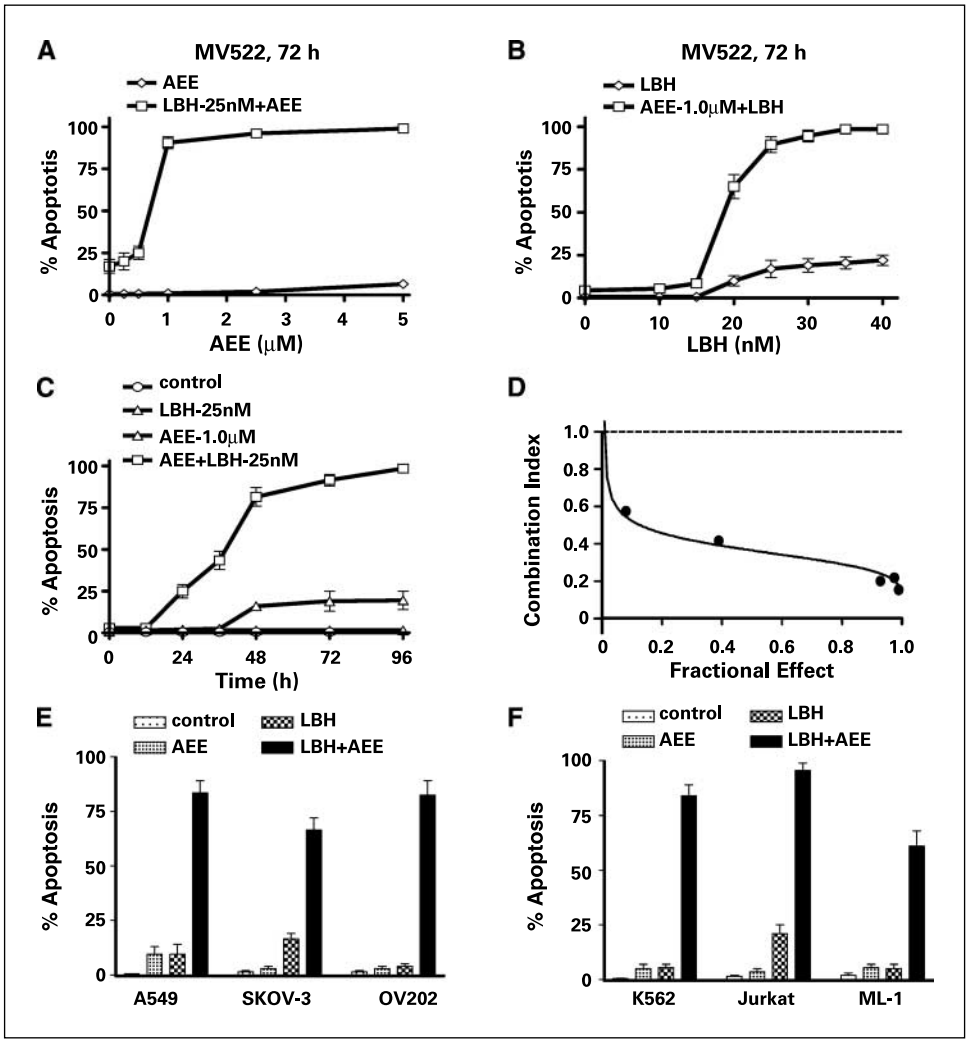

Fig. 2. Synergistic cell killing in solid cancer and leukemia cell lines by AEE788 combined with LBH589. The percentage of apoptotic cells was determined by 4′,6-diamidino-2-phenylindole dihydrochloride staining after exposure of MV522 cells for 72 h to the indicated concentrations of AEE788 with/without 25 nmol/L LBH589 (*A*), after exposure of MV522 cells for 72 h to the indicated concentrations of LBH589 with/without 1.0 μmol/L AEE788 (*B*), and after exposure of MV522 cells to 25 nmol/L LBH589 with/without 1.0 μmol/L AEE788 at indicated time intervals (*C*). MV522 cells were treated with various concentrations of LBH589 (15-45 nmol/L) and/or AEE788 (1.0-3.0 μmol/L) at a fixed ratio of 1:66.7. After the percentage of apoptotic cells was determined in each condition, the combination index was calculated as described in Materials and Methods (*D*). A combination index < 1 represents synergism. The percentage of apoptotic cells was determined by 4′,6-diamidino-2-phenylindole dihydrochloride staining after exposure of A549, SKOV-3, or OV202 cells (*E*), or by Wright-Giemsa staining after exposure of K562, Jurkat, or ML-1 cells (*F*). Conditions are as follows: A549, 72 h, AEE788 (5.0 μmol/L), LBH589 (25 nmol/L); SKOV-3, 72 h, AEE788 (5.0 μmol/L), LBH589 (20 nmol/L); OV202, 120 h, AEE788 (5 μmol/L), LBH589 (20 nmol/L); K562, 24 h, AEE788 (2.5 μmol/L), LBH589 (25 nmol/L); Jurkat or ML-1, 48 h, AEE788 (1.0 μmol/L), LBH589 (15 nmol/L). Points/columns, means for three replicate determinations; bars, SD.

plasmid using standard techniques. Both the entire green fluorescent protein (GFP)/MEK1 and GFP/Akt1 cDNAs in the fusion construct were sequenced, and the reading frames were confirmed. Log-phase A549 cells were transfected with a pEGFP empty vector, a pEGFP/MEK1 or a pEGFP/Akt1 fusion plasmid using LipofectAMINE Plus (Invitrogen, Frederick, MD) following the supplier's instructions. After a 24-h incubation, 50% to 60% of the cells displayed green fluorescence. The brightest 30% to 40% of the total cell population was isolated by fluorescence-activated cell sorting and analyzed as described in the text.

Statistical analysis. All of the data were expressed as mean ± SD from three individual experiments. Differences between groups were determined by using the Student's *t* test for unpaired observations. $P < 0.05$ was considered significant.

Results

Induction of enhanced cell death in MV522 and K562 cells after exposure to AEE788 and LBH589. Previous *in vitro* and *in vivo* studies have shown that AEE788 inhibits multiple receptor tyrosine kinases, including EGFR, HER-2, and VEGFR, as well as their downstream targets MAPK and Akt (1–4). Additional studies have shown that inhibition of MAPK potentiates HDAC inhibitor–induced apoptosis, and constitutive activation of MAPK protects against HDAC inhibitor–induced cell death (35, 36). Thus, we set out to determine whether concomitant exposure of cancer cells to AEE788 and HDAC inhibitors (e.g., LBH589) would result in enhanced induction of apoptosis. MV522 non–small cell lung cancer and K562 chronic myelogenous leukemia cells were treated with LBH589 or AEE788 alone, or in combination. LBH589 or AEE788 alone was minimally toxic, but the combination yielded a marked increase in cell death (>75%) as seen in Fig. 1A and B.

Synergistic cytotoxicity and leukemia of the combination of AEE788 and LBH589 in solid tumor and leukemia cell lines. To gain further insight into this interaction in MV522 cells, dose-response, time course, and combination index studies were done for AEE788, LBH589, and AEE788 combined with LBH589. Although exposure of MV522 cells to either 25 nmol/L LBH589 or the indicated concentrations of AEE788 alone for 72 h did not induce significant cytotoxicity, the combination resulted in a marked increase in apoptosis, with the peak of cell death occurring at 1 μmol/L AEE788 (Fig. 2A). Similarly, MV522 cells were treated with 1.0 μmol/L AEE788 either with or without graded concentrations of LBH589. Again, neither LBH589 nor AEE788 alone induced significant

cytotoxicity, but the combination yielded a marked increase in apoptosis, with the peak of cell death observed at an LBH589 concentration of 25 nmol/L (Fig. 2B). These data show a dose-dependent increase in the amount of apoptosis caused by the combination of LBH589 and AEE788 in MV522 cells. Time course studies were also done in MV522 cells by exposing cells to 25 nmol/L LBH589 with or without 1.0 μmol/L AEE788 for the indicated time intervals, and the results show that the induction of apoptosis is time dependent. Maximum apoptosis occurred at 72 h (Fig. 2C). To formally examine the synergistic interaction of the combination of AEE788 and LBH589, MV522 cells were treated with varying concentrations of LBH589 and AEE788 at a fixed ratio, and the combination index values for apoptosis induction were determined using the median effect method of Chou and Talalay (44). As shown in Fig. 2D, the combination index values were <1, indicating a synergistic interaction.

To confirm that the interaction of LBH589 and AEE788 seen in MV522 cells were not cell line specific, we further characterized the combination in other cancer cell lines. Again, this synergistic cytotoxic interaction was shown in other solid tumor cell lines, including A549 non–small cell lung cancer, SKOV-3 ovarian cancer, OV202hp cisplatin-resistant human ovarian cancer (Fig. 2E), and K562, Jurkat, and ML-1 leukemia (Fig. 2F).

To test whether the synergistic interaction between LBH589 and AEE788 extended to combinations of AEE788 and other HDAC inhibitors, MV522 cells were treated with AEE788 and/or the HDAC inhibitors LAQ824 or trichostatin A for 72 h. A marked enhancement of apoptosis occurred when AEE788 was combined with either LAQ824 or trichostatin A (data not shown), suggesting that the synergism is an HDAC inhibitor class effect and not specific for LBH589.

Effects of the combination of AEE788 and LBH589 on signaling pathways. To confirm the induction of apoptosis by this combination, we analyzed biological markers of apoptosis from cell extracts of MV522 and SKOV-3. The combination resulted in marked cleavage of procaspase-9, procaspase-3, procaspase-8, Bid, and PARP, whereas the individual agents did not (Fig. 3A). The combination also induced release of cytochrome *c* from mitochondria (Fig. 3A).

To elucidate the mechanistic basis for the synergistic cytotoxicity between LBH589 and AEE788, we determined the effects of this combination on various intracellular signaling and apoptosis-regulatory proteins in MV522 and SKOV-3 cells (Fig. 3B). In both cell lines, LBH589 treatment resulted in the predicted histone H3 and H4 acetylation as well as increased p21 expression. Combining AEE788 with LBH589 did not modify these molecular events (Fig. 3B). AEE788 treatment resulted in decreased phosphorylation of Erk1/2, Akt, glycogen synthase kinase-3β, and p70S6K at an early time point (16 h), when there was no significant induction of apoptosis (Fig. 2), and PARP was not cleaved (Fig. 3A). In addition, phosphorylation of Erk1/2 and Akt were blocked by AEE788 and its combination with LBH589 in A549 cells (Fig. 3C) as well as in H1650 and H1703 non–small cell lung cancer cells (data not shown). This abrogation of Erk1/2 and Akt activation by AEE788 treatment is consistent with previous reports in which AEE788 blocked phosphorylated Erk1/2 and phosphorylated Akt *in vitro* and *in vivo* (2, 4). It was also previously shown that inactivation of MAPK and PI3K cascades enhances HDAC inhibitor–induced apoptosis in solid tumors and leukemia cells (35–37).

MAPK or Akt protects cells from apoptosis induced by LBH589 alone or the combination of LBH589 and AEE788. To better understand whether blockage of Erk1/2 and Akt cascades by AEE788 contributes to LBH589-induced apoptosis, we used pharmacologic and genetic tools to perturb these pathways. First, A549 cells were exposed to LBH589 in the presence or absence of pharmacologic inhibitors of MEK (U0126) and/or PI3K (LY294002) under the indicated conditions (Fig. 4A). Although inhibition of MEK by U0126, PI3K/Akt by LY294002, or concomitant inhibition of MEK and PI3K/Akt by U0126 +

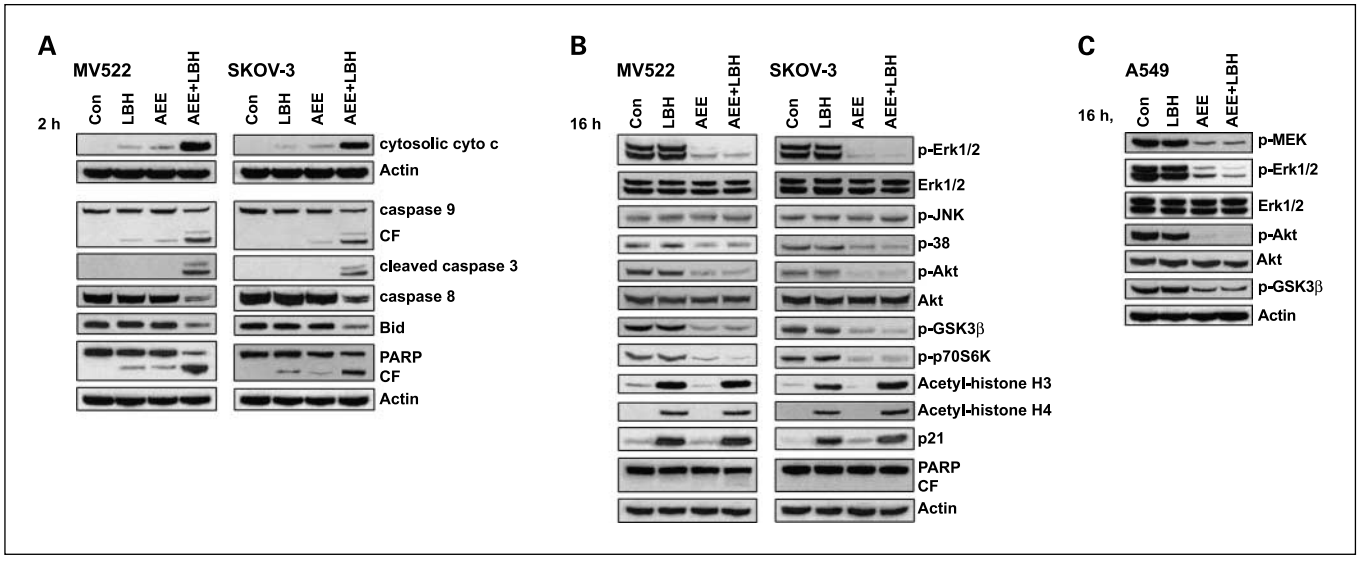

Fig. 3. Effects of the AEE788/LBH589 combination on signaling pathways. *A,* after MV522 or SKOV-3 cells were treated with control medium, LBH589 alone, AEE788 alone, or the combination for 72 h, protein extracts were analyzed by Western blotting for caspase-9, cleaved caspase-3, caspase-8, or PARP in whole-cell lysates, and cytochrome *c* (*cyto c*) from the cytosolic fraction. The drug concentrations were as follows: MV522 (25 nmol/L LBH589, 2.5 μmol/L AEE788) and SKOV-3 (20 nmol/L LBH589, 5.0 μmol/L AEE788). MV522 or SKOV-3 cells (*B*) or A549 cells (*C*) were treated for 16 h as in (*A*). Whole-cell lysates were prepared for immunoblotting with reagents that recognize the indicated antigens. CF, cleaved fragment.

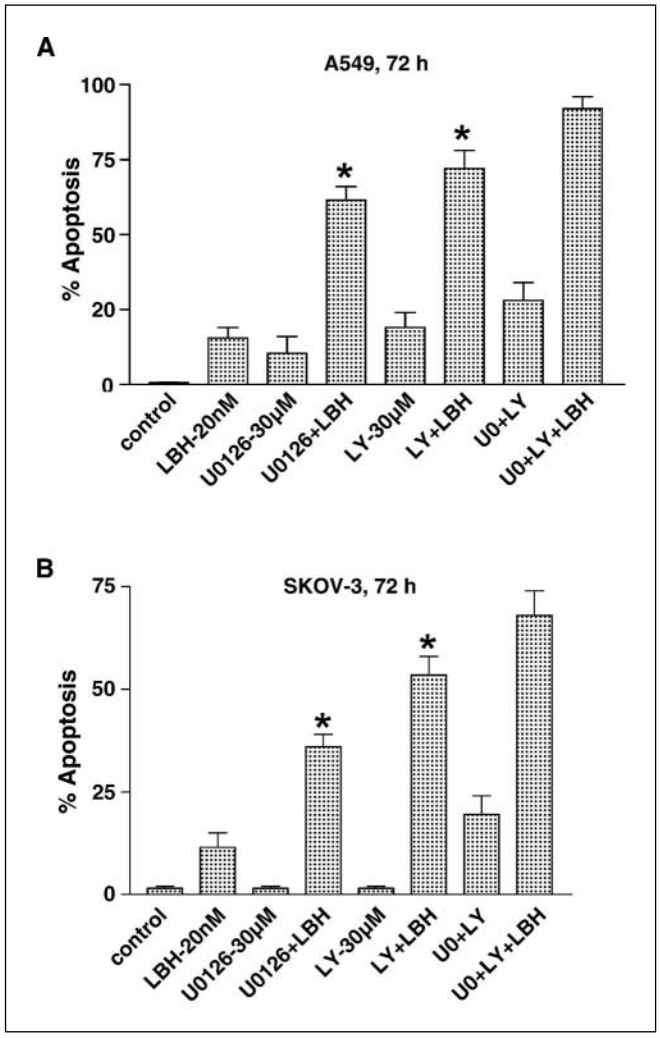

Fig. 4. MAPK or Akt protects cells from LBH589 alone or in combination with AEE788-induced apoptosis. The percentage of apoptotic cells was determined by 4′,6-diamidino-2-phenylindole dihydrochloride staining in A549 (*A*) or SKOV-3 cells (*B*) after exposure of cells to the indicated conditions. Columns, means for three replicate determinations; bars, SD. *, $P < 0.05$, relative to cells treated with the combination of U0126 (*U0*), LY294002 (*LY*), and LBH589.

LY294002 elicited modest cytotoxicity, inhibition of either MEK or PI3K/Akt potentiated LBH589-induced apoptosis. Concomitant inhibition of MEK and PI3K/Akt by U0126 + LY294002 significantly enhanced LBH589-induced apoptosis in comparison with inhibition of either pathway (MEK or Akt) individually, suggesting that abrogation of Erk1/2 and Akt signals by AEE788 does contribute to LBH589-induced apoptosis. Similar results were obtained in another type of cancer cell line, SKOV-3 (Fig. 4B).

To validate these results without pharmacologic inhibitors, A549 cells were transiently transfected with GFP-tagged, constitutively active MEK1 (CA-MEK1). GFP-tagged cells were then isolated by fluorescence-activated cell sorting. Cells with GFP/CA-MEK1 were more resistant to LBH589-induced apoptosis in a dose-dependent manner than cells transfected with GFP only (Fig. 5A). In addition, CA-MEK1 also protected cells from LBH589 + AEE788 – induced apoptosis. Only about 40% of the A549 cells expressing CA-MEK1 became apoptotic after LBH589 + AEE788 treatment, compared with about 65% of cells expressing GFP alone (Fig. 5B). Results in Fig. 5C further confirmed two observations. First, the GFP/CA-MEK1 activated the MEK pathway, as shown by the detection of increased levels of phosphorylated Erk1/2. Second, apoptosis in cells expressing CA-MEK1 was blocked as detected by decreased PARP cleavage, which is a biochemical hallmark of apoptosis.

To determine whether inhibition of Akt signaling by AEE788 is involved in LBH589- or LBH589 + AEE788 – induced apoptosis, A549 cells were likewise transfected with GFP-tagged, constitutively active Akt1 (CA-Akt1). Once again, significant protection from cell death was observed when apoptosis evaluated by nuclear morphology and PARP cleavage in CA-Akt1 cells after treatment with LBH589 alone or LBH589 + AEE788 (Fig. 5D and E). The function of the CA-Akt1 construct was monitored by enhancement of phosphorylated glycogen synthase kinase-3β levels (Fig. 5F). Comparatively, the level of protection in cells expressing CA-MEK1 is slightly greater than in cells with CA-Akt1. Taken together, these results show that both the MAPK and Akt pathways can protect cancer cells from LBH589- or LBH589 + AEE788 – induced apoptosis.

Induction of enhanced ROS generation is correlated to induction of enhanced apoptosis in cancer cells after exposure to a combination of AEE788 and LBH589. It has been reported that HDAC inhibitor – induced cytotoxicity is associated with generation of ROS (17), and that the MAPK pathway plays a role in protecting cells from oxidative stress (45). Thus, we next examined whether blockade of the Erk pathway by AEE788 enhances the capacity of HDAC inhibitors to generate ROS. K562 cells were treated with LBH589 and/or AEE778. Although LBH589 or AEE788 alone did not significantly induce the generation of ROS, the combination induced a marked increase in ROS (Fig. 6A and B). Moreover, free radical scavenger *N*-acetyl-L-cysteine not only substantially suppressed the ROS accumulation but also completely blocked the cleavage of caspase-3 and PARP as well as inhibited the induction of apoptosis by the combination treatment. Conversely, the pan-caspase inhibitor BOC-fmk did not significantly prevent the combination-generated ROS ($P > 0.05$; Fig. 6B), but did block cytochrome *c* release, caspase activation and apoptosis (data now shown), indicating that ROS induction is the upstream event of caspase activation and apoptosis. These results indicate that AEE788 promotes LBH589-mediated generation of ROS in tumor cells, which in turn increases apoptosis. The results suggest a model in which inhibition of multiple survival pathways may shift the balance of intracellular events towards apoptosis. The molecular mechanism through which the Erk or Akt pathways regulate the production of ROS remains to be defined.

Discussion

In the present study, we have shown synergistic cytotoxicity when the multi-kinase inhibitor AEE788 is combined with the HDAC inhibitor LBH589, LAQ824, or trichostatin A in multiple solid tumor and leukemia cell lines as well as in cisplatin-resistant ovarian cancer cells. Using the pharmacologic inhibitors of MEK (U0126) and PI3K (LY294002), we found that inhibition of Erk1/2 or Akt potentiates HDAC inhibitor – induced apoptosis. Inhibition of both MEK and Akt pathways further enhanced HDAC inhibitor – induced cell death in comparison with that seen with inhibition of either pathway

alone. In contrast, apoptosis was attenuated when LBH589 or the combination of LBH589 and AEE788 was used in cells overexpressing a constitutively active form of either MEK1 or Akt1. These results suggest that abrogation of MAPK and Akt signaling cascades by AEE788 is obligatory for the synergistic cytotoxicity resulting from the combination of AEE788 and HDAC inhibitors.

We propose that the inactivation Erk1/2 and Akt account for the high incidence of apoptosis in tumor cells exposed simultaneously to LBH589 and AEE788. A number of findings support this hypothesis. First, inactivation of Erk1/2 by MEK inhibitor U0126 enhances HDAC-induced apoptosis. Second, Akt is the major effector of the activated PI3K pathway, and its inactivation by the PI3K inhibitor LY294002 enhanced the sensitivity of cells to HDAC inhibitor–induced apoptosis. Most importantly, cells with constitutively active MEK1 or Akt1 showed an attenuated apoptotic response to the combination of LBH589 and AEE788.

Increased ROS generation is another mechanism that can underlie the observed synergistic effects of AEE788 in combination with HDAC inhibitors. HDAC inhibitors have been shown to kill cells by ROS induction (46–48), and inhibition of MAPK enhances HDAC inhibitor–induced cell death by promoting ROS production (35, 36). ROS may act directly on the mitochondria, inducing the mitochondrial membrane permeability transition and resulting in the release of apoptogenic factors, such as cytochrome *c*, apoptosis-inducing factor, and/or Smac/DIABLO (21, 22, 24–27). Earlier studies indicate that inhibition of the MEK pathway enhances HDAC inhibitor–induced apoptosis in chronic myelogenous leukemia via increased induction of ROS and prevention of p21 expression (35). Conversely, active Erk1/2 protects cells from multiple stimulus-induced cell death mechanisms, including ROS generation (36). Our present study indicates that concomitant exposure to AEE788 and LBH589 increases ROS induction, and removal of ROS by the free radical scavenger *N*-acetyl-L-cysteine completely blocks apoptosis induced by the combination, suggesting that apoptosis induction by LBH589 combined with AEE788 is correlated to ROS generation. Thus, cotreatment of cells with AEE788 and LBH589 not only increases the generation of ROS but also blocks the cytoprotective response of cells. It is possible that blocking multiple survival pathways may tip the balance of intracellular events toward apoptosis. It remains unclear, however, how the abrogation of MAPK and Akt causes increased ROS production.

AEE788 and LBH589 are currently in phase I clinical development. Previous studies *in vitro* and *in vivo* indicate that AEE788 inhibits multiple receptor tyrosine kinases, including EGFR, HER-2, and VEGFR, as well as downstream targets MAPK and Akt (2–4). Abnormalities within these cellular components are frequently found in a variety of tumor types, including ovarian, lung, and breast cancer. To provide insights

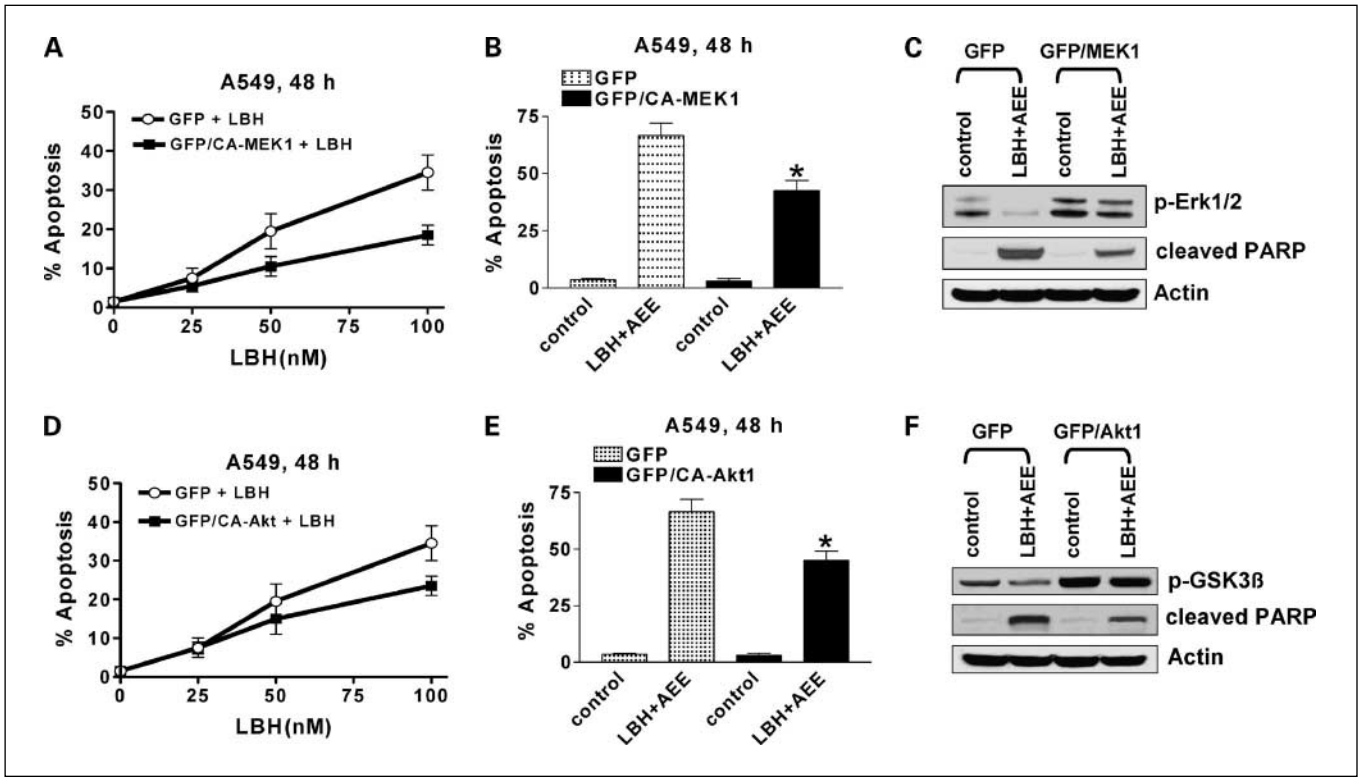

Fig. 5. Constitutively active MEK or Akt protects against apoptosis induced by LBH589 and AEE788. A549 cells were transiently transfected with plasmids encoding GFP or a constitutively active MEK1 construct fused to GFP, incubated overnight to allow transgene expression, and then sorted based on GFP fluorescence. GFP-positive cells in each condition were treated with indicated concentrations of LBH589 (*A*), or 25 nmol/L LBH589 + 5.0 μmol/L AEE788 (*B*) for 48 h and then assayed for extent of apoptosis morphologically. Some cells were harvested for analysis of phosphorylated Erk1/2 (*p-Erk1/2*) and PARP by immunoblotting (*C*). A549 cells were transiently transfected with plasmids encoding GFP or a constitutively active Akt1 construct fused to GFP, incubated overnight to allow transgene expression, and then sorted based on GFP fluorescence. GFP-positive cells in each condition were treated with indicated concentrations of LBH589 (*D*), or 25 nmol/L LBH589 + 5.0 μmol/L AEE788 (*E*) for 48 h and then assayed for extent of apoptosis morphologically. Some cells were harvested for analysis of phosphorylated glycogen synthase kinase-3β (*p-GSK3β*) and PARP by immunoblotting (*F*).

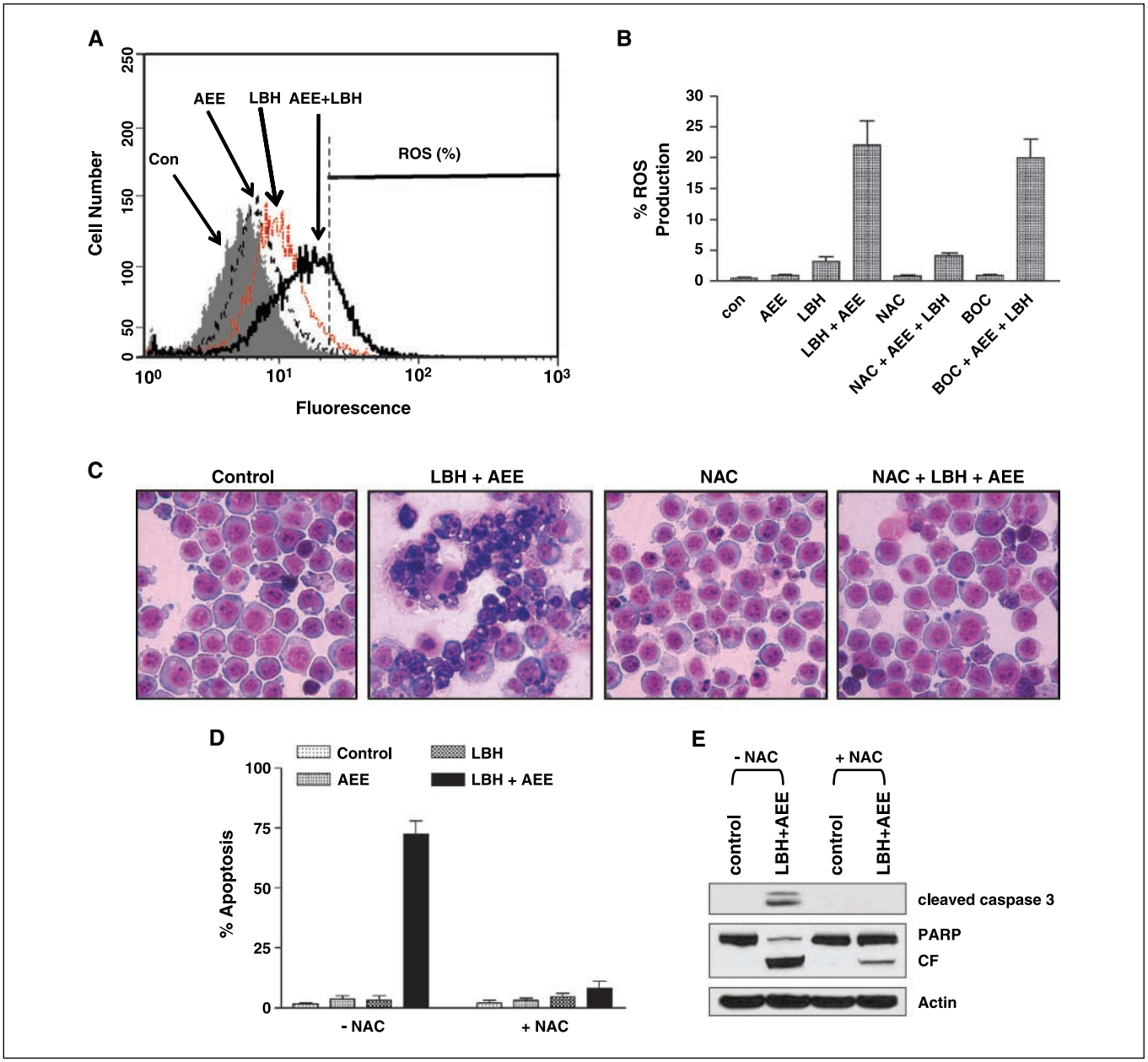

Fig. 6. ROS generation is correlated to apoptosis induction. *A,* after exposure of K562 cells to AEE788 with/without LBH589 for 12 h, ROS generation was determined by flow cytometry, reflected by the rightward shift of the histogram. *B,* the percentage of with significant ROS generation was analyzed by flow cytometry in the conditions as indicated. *C,* after K562 cells were treated as indicated conditions for 24 h, apoptosis was determined morphologically by Wright-Giemsa staining. *D,* after K562 cells were treated as indicated conditions, the percentage of apoptosis cells were determined by microscope with Wright-Giemsa staining. *E,* Western analysis of cleaved caspase-3 and PARP was done after exposure of K562 cells to LBH589 + LBH589 for 24 h. Reagent concentrations at above experiments are as follows: AEE788, 2.5 μmol/L; LBH589, 25 nmol/L; *N*-acetyl-L-cysteine (*NAC*), 12 mmol/L; BOC, 50 μmol/L.

for future clinical application, we further explored this combination regimen in cisplatin-resistant ovarian tumors. Ovarian cancer is the leading gynecologic malignancy. These tumors are often initially sensitive to platinum-based chemotherapy, but resistance commonly develops; therefore, recurrence is a major clinical challenge for ovarian cancer patients after chemotherapy. Our data suggest that that there is synergistic cytotoxicity in OV202hp cells after exposure to the combination of LBH589 and AEE788 (Fig. 2E). Notably, the major changes in signaling events seen in cell lines (MV522 and SKOV-3; Fig. 3B), including decreased phosphorylated Erk1/2 and phosphorylated Akt, were observed in the cisplatin-resistant human ovarian tumor cells, OV202hp (data not shown). Importantly, neither AEE nor LBH589, alone or in combination, showed significant cytotoxicity against normal peripheral blood mononuclear cells (data not shown), suggesting that this combination may have limited toxicity against nontransformed cells. These findings suggest the possibility of testing of an LBH589 + AEE788 combination regimen in recurrent ovarian cancer patients after platinum-based chemotherapy.

Because numerous survival pathways are activated in transformed cells and form redundant signal transduction

networks that interact with each other, interruption of merely one pathway is likely to be insufficient to induce cell death or growth arrest, as other pathways may be able to compensate and promote tumor cell survival. An effective cancer therapy is one that can interrupt multiple crucial survival pathways and shift the balance of intracellular events toward death. The above results suggest that the inhibition of MEK and Akt signaling could be a potent approach to substantially enhance the antitumor effects of HDAC inhibitors. The combination of AEE788 with LBH589 shows synergism in refractory cancer cell lines (i.e., lung, ovarian, and chronic myelogenous leukemia) as well as in cisplatin-resistant ovarian cancer cells. Consequently, this combination provides a promising potential for additional preclinical and possible clinical evaluation.

Acknowledgments

We thank Drs. Robert Jenkins and Keith C. Bible (Mayo Clinic, Rochester, MN) for kindly providing OV202hp cells used in this research.

References

1. Traxler P, Allegrini PR, Brandt R, et al. AEE788: a dual family epidermal growth factor receptor/ErbB2 and vascular endothelial growth factor receptor tyrosine kinase inhibitor with antitumor and antiangiogenic activity. Cancer Res 2004;64:4931–41.
2. Park YW, Younes MN, Jasser SA, et al. AEE788, a dual tyrosine kinase receptor inhibitor, induces endothelial cell apoptosis in human cutaneous squamous cell carcinoma xenografts in nude mice. Clin Cancer Res 2005;11:1963–73.
3. Yazici S, Kim SJ, Busby JE, et al. Dual inhibition of the epidermal growth factor and vascular endothelial growth factor phosphorylation for antivascular therapy of human prostate cancer in the prostate of nude mice. Prostate 2005;65:203–15.
4. Yokoi K, Thaker PH, Yazici S, et al. Dual inhibition of epidermal growth factor receptor and vascular endothelial growth factor receptor phosphorylation by AEE788 reduces growth and metastasis of human colon carcinoma in an orthotopic nude mouse model. Cancer Res 2005;65:3716–25.
5. Brunet A, Pouyssegur J. Mammalian MAP kinase modules: how to transduce specific signals. Essays Biochem 1997;32:1–16.
6. Widmann C, Gibson S, Jarpe MB, Johnson GL. Mitogen-activated protein kinase: conservation of a three-kinase module from yeast to human. Physiol Rev 1999;79:143–80.
7. Xia Z, Dickens M, Raingeaud J, Davis RJ, Greenberg ME. Opposing effects of ERK and JNK-p38 MAP kinases on apoptosis. Science (Washington DC) 1995;270:1326–31.
8. Seger R, Krebs EG. The MAPK signaling cascade. FASEB J 1995;9:726–35.
9. Lewis TS, Shapiro PS, Ahn NG. Blockade of the ERK pathway markedly sensitizes tumor cells to HDAC inhibitor-induced cell death. Adv Cancer Res 1998;74:149–59.
10. Friday BB, Adjei AA. K-*ras* as a target for cancer therapy. Biochim Biophys Acta 2005;1756:127–44.
11. Xing M. BRAF mutation in thyroid cancer. Endocr Relat Cancer 2005;12:245–62.
12. Haluska FG, Tsao H, Wu H, Haluska FS, Lazar A, Goel V. Genetic alterations in signaling pathways in melanoma. Clin Cancer Res 2006;12:2301–7s.
13. Nicholson K, Anderson NG. The protein kinase B/Akt signalling pathway in human malignancy. Cell Signal 2002;14:381–95.
14. Wolffe AP, Guschin D. Review: chromatin structural features and targets that regulate transcription. J Struct Biol 2000;129:102–22.
15. Marks P, Rifkind RA, Richon VM, Breslow R, Miller T, Kelly WK. Histone deacetylases and cancer: causes and therapies. Nat Rev Cancer 2001;1:194–202.
16. Rosato RR, Wang Z, Gopalkrishnan RV, Fisher PB, Grant S. Evidence of a functional role for the cyclin-dependent kinase-inhibitor p21WAF1/CIP1/MDA6 in promoting differentiation and preventing mitochondrial dysfunction and apoptosis induced by sodium butyrate in human myelomonocytic leukemia cells (U937). Int J Oncol 2001;19:181–91.
17. Ruefli AA, Ausserlechner MJ, Bernhard D, et al. The histone deacetylase inhibitor and chemotherapeutic agent suberoylanilide hydroxamic acid (SAHA) induces a cell-death pathway characterized by cleavage of Bid and production of reactive oxygen species. Proc Natl Acad Sci U S A 2001;98:10833–53.
18. Thannickal VJ, Fanburg BL. Reactive oxygen species in cell signaling. Am J Physiol Lung Cell Mol Physiol 2000;279:L1005–28.
19. Balaban RS, Nemoto S, Finkel T. Mitochondria, oxidants, and aging. Cell 2005;120:483–95.
20. Fiers W, Beyaert R, Declercq W, Vandenabeele P. More than one way to die: apoptosis, necrosis and reactive oxygen damage. Oncogene 1999;18:7719–30.
21. Susin SA, Lorenzo HK, Zamzami N, et al. Molecular characterization of mitochondrial apoptosis-inducing factor. Nature 1999;397:441–6.
22. Kroemer G, Reed JC. Mitochondrial control of cell death. Nat Med 2000;6:513–9.
23. Cregan SP, Dawson VL, Slack RS. Role of AIF in caspase-dependent and caspase-independent cell death. Oncogene 2004;23:2785–96.
24. Du C, Fang M, Li Y, Li L, Wang X. Smac, a mitochondrial protein that promotes cytochrome *c*-dependent caspase activation by eliminating IAP inhibition. Cell 2000;102:33–42.
25. Li P, Nijhawan D, Budihardjo I, et al. Cytochrome *c* and dATP-dependent formation of Apaf-1/caspase-9 complex initiates an apoptotic protease cascade. Cell 1997;91:479–89.
26. Li LY, Luo X, Wang X. Endonuclease G is an apoptotic DNase when released from mitochondria. Nature 2001;412:95–9.
27. Wang X. The expanding role of mitochondria in apoptosis. Genes Dev 2001;15:2922–33.
28. Nakata S, Yoshida T, Horinaka M, Shiraishi T, Wakada M, Sakai T. Histone deacetylase inhibitors upregulate death receptor 5/TRAIL-R2 and sensitize apoptosis induced by TRAIL/APO2-L in human malignant tumor cells. Oncogene 2004;23:6261–71.
29. Insinga A, Monestiroli S, Ronzoni S, et al. Inhibitors of histone deacetylases induce tumor-selective apoptosis through activation of the death receptor pathway. Nat Med 2005;11:71–6.
30. Nebbioso A, Clarke N, Voltz E, et al. Tumor-selective action of HDAC inhibitors involves TRAIL induction in acute myeloid leukemia cells. Nat Med 2005;11:77–84.
31. Yu X, Guo ZS, Marcu MG, et al. Modulation of p53, ErbB1, ErbB2, and Raf-1 expression in lung cancer cells by depsipeptide FR901228. J Natl Cancer Inst 2002;94:504–13.
32. Singh TR, Shankar S, Srivastava RK. HDAC inhibitors enhance the apoptosis-inducing potential of TRAIL in breast carcinoma. Oncogene 2005;24:4609–23.
33. Qian DZ, Kato Y, Shabbeer S, et al. Targeting tumor angiogenesis with histone deacetylase inhibitors: the hydroxamic acid derivative LBH589. Clin Cancer Res 2006;12:634–42.
34. Beck J, Fischer T, Rowinsky E, et al. Phase I pharmacokinetic and pharmacodynamic study of LBH589: A novel histone deacetylase inhibitor. J Clin Oncol 2004;22:3025.
35. Yu C, Dasmahapatra G, Dent P, Grant S. Synergistic interactions between MEK1/2 and histone deacetylase inhibitors in BCR/ABL$^+$ human leukemia cells. Leukemia 2005;19:1579–89.
36. Ozaki K, Minoda A, Kishikawa F, Kohno M. Blockade of the ERK pathway markedly sensitizes tumor cells to HDAC inhibitor-induced cell death. Biochem Biophys Res Commun 2006;339:1171–7.
37. Denlinger CE, Rundall BK, Jones DR. Inhibition of phosphatidylinositol 3-kinase/Akt and histone deacetylase activity induces apoptosis in non-small cell lung cancer *in vitro* and *in vivo*. J Thorac Cardiovasc Surg 2005;130:1422–9.
38. Yu C, Rahmani M, Almenara J, et al. Histone deacetylase inhibitors promote STI571-mediated apoptosis in STI571-sensitive and -resistant Bcr/Abl$^+$ human myeloid leukemia cells. Cancer Res 2003;63:2118–26.
39. Nimmanapalli R, Fuino L, Stobaugh C, Richon V, Bhalla K. Cotreatment with the histone deacetylase inhibitor suberoylanilide hydroxamic acid (SAHA) enhances imatinib-induced apoptosis of Bcr-Abl-positive human acute leukemia cells. Blood 2003;101:3236–9.
40. Yu C, Rahmani M, Conrad D, Subler M, Dent P, Grant S. The proteasome inhibitor bortezomib interacts synergistically with histone deacetylase inhibitors to induce apoptosis in Bcr/Abl$^+$ cells sensitive and resistant to STI571. Blood 2003;102:3765–74.
41. Catley L, Weisberg E, Kiziltepe T, et al. Aggresome induction by proteasome inhibitor bortezomib and {alpha}-tubulin hyperacetylation by tubulin deacetylase (TDAC) inhibitor LBH589 are synergistic in myeloma cells. Blood 2006;108:3441–9.
42. Varki NM, Estes LA, Tseng A, Vu TP. Spontaneously metastasizing variants of a human lung carcinoma cell line: monoclonal antibody characterization. Tumour Biol 1990;11:327–38.
43. Bible KC, Boerner SA, Kirkland K, et al. Characterization of an ovarian carcinoma cell line resistant to cisplatin and flavopiridol. Clin Cancer Res 2000;6:661–70.
44. Chou TC, Talalay P. Quantitative analysis of dose-effect relationships: the combined effects of multiple drugs or enzyme inhibitors. Adv Enzyme Regul 1984;22:27–55.
45. Adjei AA, Davis JN, Bruzek LM, Erlichman C, Kaufmann SH. Synergy of the protein farnesyltransferase inhibitor SCH66336 and cisplatin in human cancer cell lines. Clin Cancer Res 2001;7:1438–45.
46. Wang X, Martindale JL, Liu Y, Holbrook NJ. Endogenously produced lipoprotein lipase enhances the binding and cell association of native, mildly oxidized and moderately oxidized low-density lipoprotein in mouse peritoneal macrophages. Biochem J 1999;343:347–53.
47. Rosato RR, Almenara JA, Grant S. The histone deacetylase inhibitor MS-275 promotes differentiation or apoptosis in human leukemia cells through a process regulated by generation of reactive oxygen species and induction of p21CIP1/WAF1 1. Cancer Res 2003;63:3637–45.
48. Ungerstedt JS, Sowa Y, Xu WS, et al. Role of thioredoxin in the response of normal and transformed cells to histone deacetylase inhibitors. Proc Natl Acad Sci U S A 2005;102:673–8.